nature nanotechnology

SUPPLEMENTARY INFORMATION

DOI: 10.1038/NNANO.2015.279

# A biomimetic DNA-based channel for the ligand-controlled transport of charged molecular cargo across a biological membrane

**Jonathan R. Burns, Astrid Seifert, Niels Fertig, Stefan Howorka**

DOI: 10.1038/NNANO.2015.279

**Contents**

## 1. DNA sequences, 2D DNA maps, and pore dimensions

### 1.1. DNA sequences

**Supplementary Table 1.** Names, chemical modifications, and sequences of DNA oligonucleotides used to prepare DNA nanopores

| ID | Sequence 5′ → 3′ |
|---|---|
| 1 | AGCGAACGTGGATTTTGTCCGACATCGGCAAGCTCCCTTTTTCGACTATT |
| 2 | CCGATGTCGGACTTTTACACGATCTTCGCCTGCTGGGTTTTGGGAGCTTG |
| 3 | CGAAGATCGTGTTTTTCCACAGTTGATTGCCCTTCACTTTTCCCAGCAGG |
| 4 | AATCAACTGTGGTTTTTCTCACTGGTGATTAGAATGCTTTTGTGAAGGGC |
| 5 | TCACCAGTGAGATTTTTGTCGTACCAGGTGCATGGATTTTTGCATTCTAA |
| 6 | CCTGGTACGACATTTTTCCACGTTCGCTAATAGTCGATTTTATCCATGCA |
| 1(chol) | Sequence of 1 carrying a cholesterol via tri(ethylene glycol) TEG linker at the 3′ end |
| 3(chol) | Sequence of 2 carrying a cholesterol via a TEG linker at the 3′ terminus |
| 4(chol) | Sequence of 4 carrying a cholesterol via a TEG linker at the 3′ terminus |
| 5(chol) | Sequence of 5 carrying a cholesterol via a TEG linker at the 3′ terminus |
| 6(chol) | Sequence of 6 carrying a cholesterol via a TEG linker at the 3′ terminus |
| 2(dock) | CCGATGTCGGACTTCGT$^{F}$GCGCTTTTAGTCACGTTACACGATCTTCGCCTGCTG GGTTTTGGGAGCTTG |
| 5(dock) | TCACCAGTGAGATTGCACGGCTTTTCGACGGATTTGTCGTACCAGGTGCATGG ATTTTTGCATTCTAA |
| lock | CACCGATCGGTGAGTAGTACGAGACGCGCACGTTTTTTTTTCCGTCGTTTTTTT TGCCGTGCTTTTTTTTCGTGACTGAGAAGAACGA |
| lock-II | CTCAT$^{T}$CGATCGGTG |
| Key | TCGTTCTTCTCAGTCACGAAAAAAAAGCACGGCAAAAAAAACGACGGAAAAAAA AACGTGCGCGTCTCGTACTA |
| mismatch key | TCGATCTATCACCGCTTGGCTATTTGGAACAGTAGGTAGAT |
| 1(short loop) | AGCGAACGTGGAGTCCGACATCGGCAAGCTCCCTCGACTATT |
| 2(short loop) | CCGATGTCGGACACACGATCTTCGCCTGCTGGGGGGAGCTTG |
| 3(short loop) | CGAAGATCGTGTCCACAGTTGATTGCCCTTCACCCCAGCAGG |
| 4(short loop) | AATCAACTGTGGTCTCACTGGTGATTAGAATGCGTGAAGGGC |
| 5(short loop) | TCACCAGTGAGATGTCGTACCAGGTGCATGGATGCATTCTAA |
| 6(short loop) | CCTGGTACGACATCCACGTTCGCTAATAGTCGAATCCATGCA |

$T^{F}$ and $T^{T}$ stand are modified nucleotides which carry the FAM and TAMRA fluorophores, respectively, at position 5 of the pyrimidine base. Due to design reason, $T^{F}$ forms a T-G mismatch with the complementary strand. Oligonucleotides 1-6 contain two $T_4$ stretches that form non-hybridizing hairpin loops at the duplex termini of the nanopores. Oligonucleotides 1-6(short loop) are of the same sequence as oligonucleotides 1-6 but lack two $T_4$ stretches.

DOI: 10.1038/NNANO.2015.279

**Supplementary Table 2.** Names and composition of DNA nanopores

| Nanopore | Oligonucleotides used |
|---|---|
| NP cholesterol-free | 1, 2, 3, 4, 5, 6 |
| NP | 1(chol), 2, 3(chol), 4, 5(chol), 6 |
| NP-C cholesterol-free | 1, 2(dock), 3, 4, 5(dock), 6, lock, lock-II |
| NP-O cholesterol-free | 1, 2(dock), 3, 4, 5(dock), 6 |
| NP-C | 1(chol), 2(dock), 3(chol), 4(chol), 5(dock), 6(chol), lock, lock-II |
| NP-O | 1(chol), 2(dock), 3(chol), 4(chol), 5(dock), 6(chol) |
| $NP_{short\ loop}$ | 1(short loop), 2(short loop), 3(short loop), 4(short loop), 5(short loop), 6(short loop) |

### 1.2. 2D maps of DNA nanopores

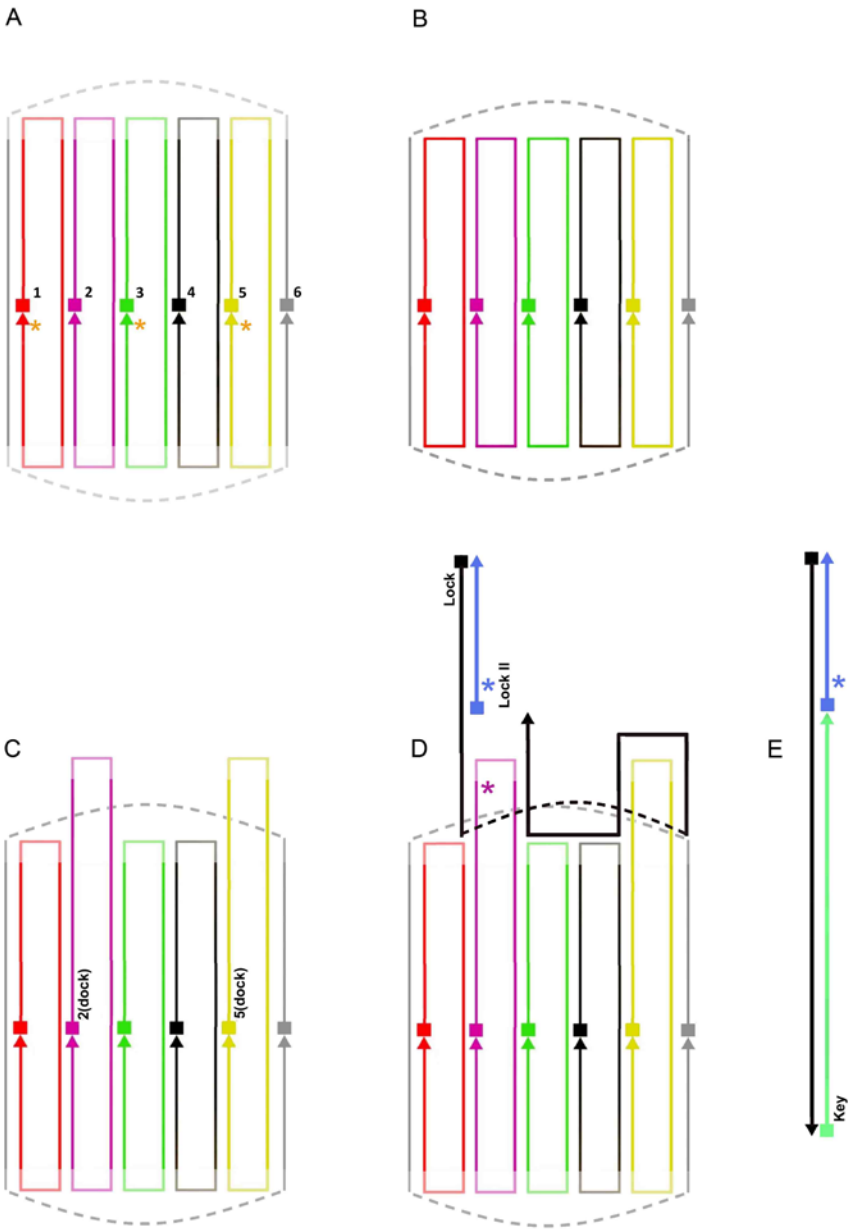


**Supplementary Fig. 1.** 2D maps of DNA nanopores (A) NP, (B) $NP_{short\ loop}$, (C) NP-O, (D) NP-C and (E) the duplex between lock, key and probe strand lock-II. The component DNA strands as represented as lines, and the 5′ and 3′ termini of the strands are indicated by squares and triangles, respectively. The $T_4$-containing hairpin loops in A, C, and D are of semi-transparent color. The positions for the cholesterol modifications are indicated by an orange asterisk. For reasons of clarity, the asterisks are only shown in panel A.

DOI: 10.1038/NNANO.2015.279

### 1.3. Dimensions of DNA nanopores

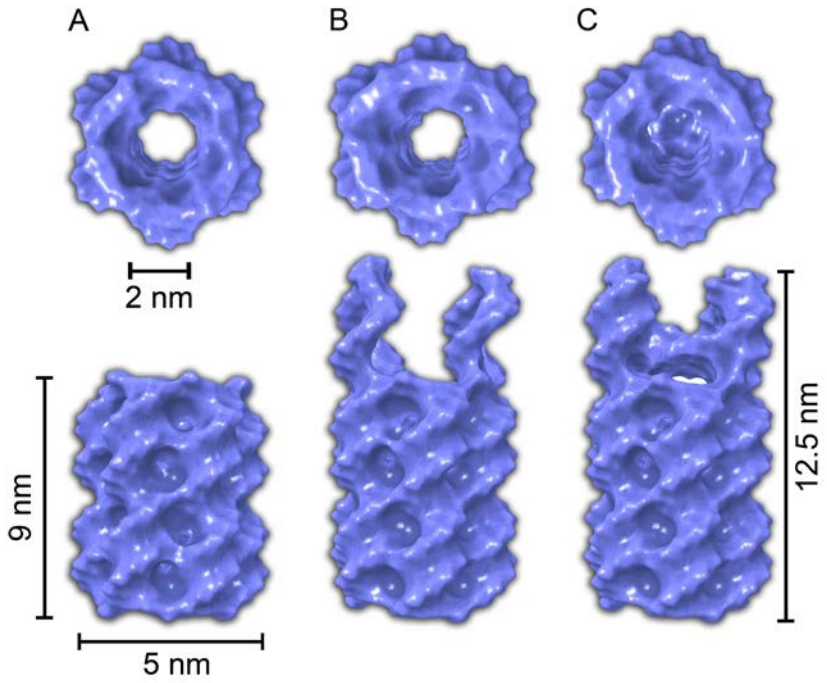


**Supplementary Fig. 2.** Space-filling models of DNA nanopores (A) NP, (B) NP-O, (C) NP-C in top and side view, and their dimensions. In NP-C there is a small gap between the lock and the upper rim of the channel wall.

## 2. Experimental results

### 2.1. Analysis of nanopores with agarose gel electrophoresis and AFM

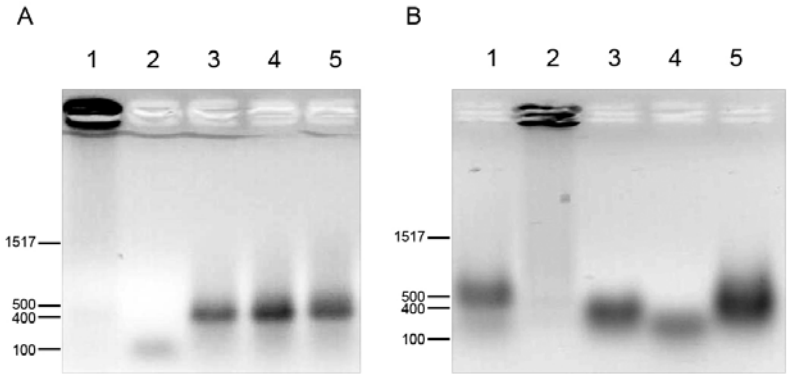


**Supplementary Fig. 3.** 1.2% Agarose gel electrophoresis of DNA nanopores and related DNA assemblies. (A) Cholesterol-free DNA nanopores folded at a rate of 20 °C per min (lane 3), 5 °C per min (lane 4), 0.5 °C per min (lane 5). Non-heated NP (lane 1) and oligonucleotide 1 (lane 2) serve as controls. (B) Non-cholesterol DNA nanopores NP (lane 1), NP with cholesterol (lane 2), cholesterol-free NP-O (lane 3) and NP-C (lane 5), and control oligonucleotide lock/lock-II (lane 4). The position and bp length of the dsDNA marker bands are indicated on the left side of each gel.

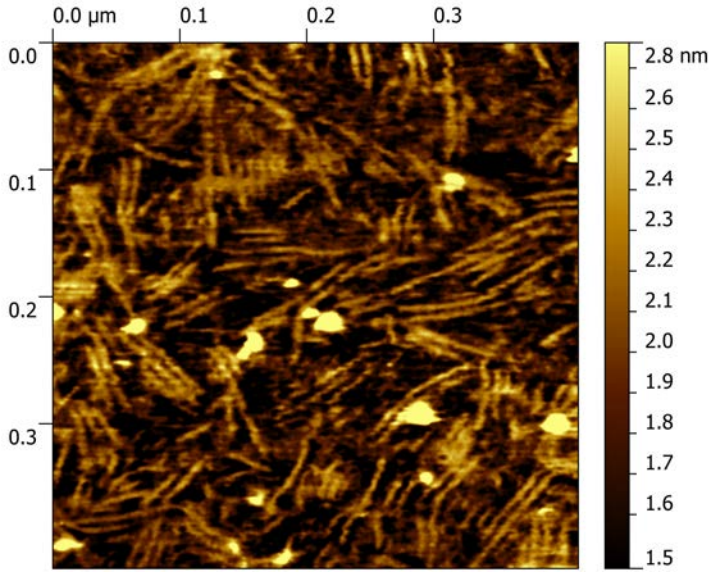


**Supplementary Fig. 4.** AFM micrograph of cholesterol-free $NP_{short\ loop}$ deposited at a concentration of 100 nM in buffer A on mica. The width, length and height of the end-to-end arranged DNA nanopore assemblies are 6.8 ± 1.2 nm, 55.0 ± 28.9 nm, and 1.3 ± 0.8 nm, respectively (n = 16).

DOI: 10.1038/NNANO.2015.279

### 2.3. UV melting profiles of DNA nanopores

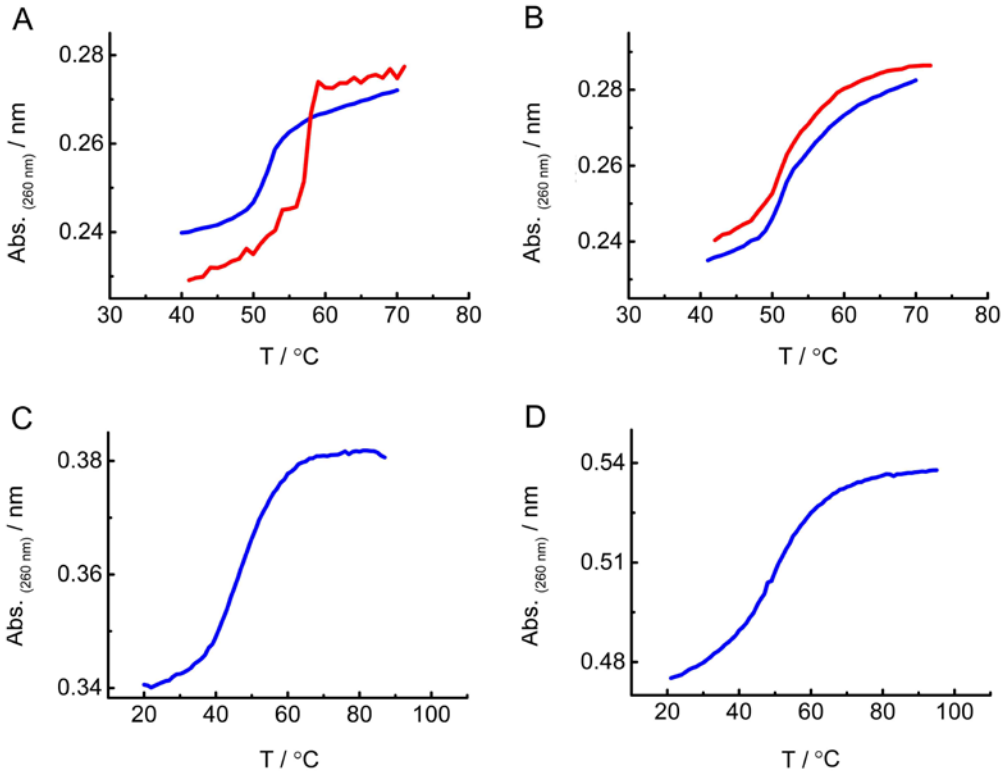


**Supplementary Fig. 5.** UV melting profiles of DNA nanopores. (A) NP with cholesterol in the absence (blue line, $T_m$ = 50.3 ± 0.7 °C) and presence of SUVs (red line, $T_m$ = 55.2 ± 0.9 °C). (B) Cholesterol-free NP in the absence (blue line; $T_m$ = 51.5 ± 0.8 °C) and presence of SUVs (red line; $T_m$ = 52.1 ± 0.7 °C), (C) cholesterol-containing NP-O ($T_m$ = 46.8 °C), (D) cholesterol-containing NP-C ($T_m$ = 49.2 °C). Samples at a concentration of 0.1 μM DNA and 500 μM lipid in buffer A were heated at a rate of 1 °C per min. The numbers in A and B represent the averages and standard deviations from three independent experiments.

### 2.4. The conductance properties of nanopore NP

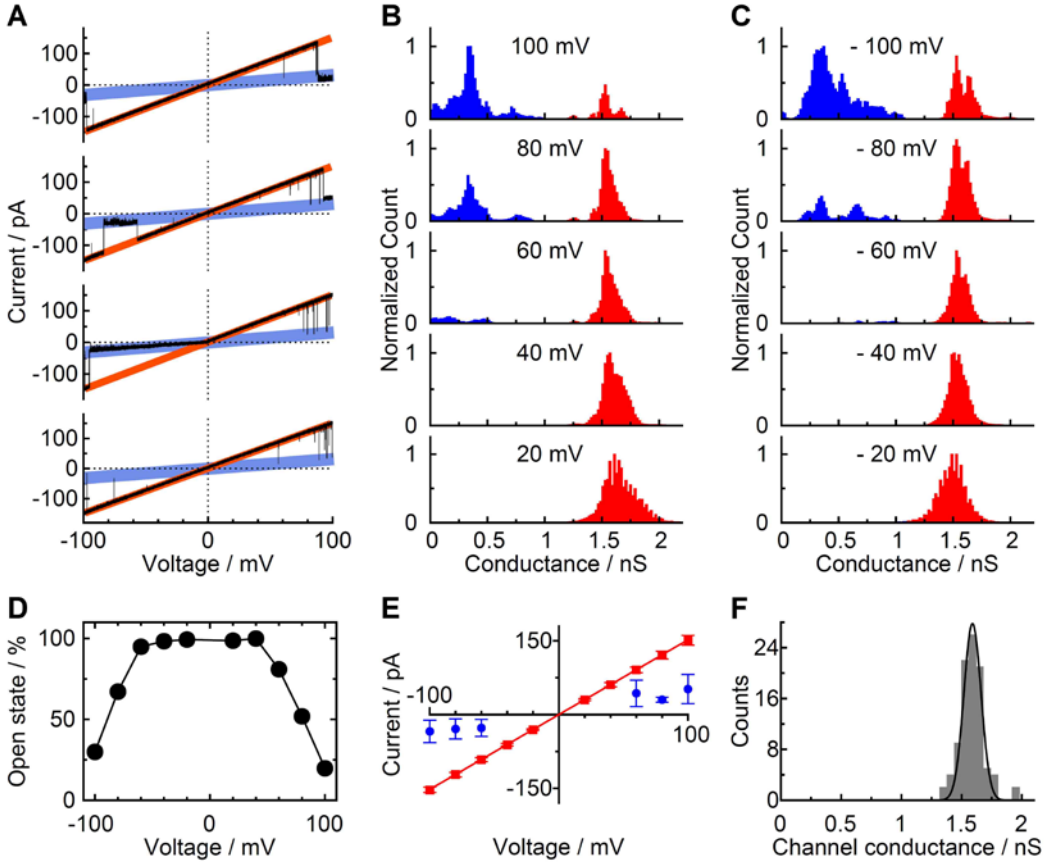


**Supplementary Fig. 6.** Single-channel current analysis of NP shows that the high-conductance (color-coded red) predominates at voltages from -60 mV to + 60 mV. Higher voltages can induce a lower conductance state (color-coded blue) which is likely caused by conformational changes in the pore structure. (A) Voltage ramps from -100 to +100 mV of single NP pores recorded in 1 M KCl, 10 mM HEPES pH 8.0. (B, C) Cumulative all-point histograms of 77 single-channel current traces for positive potentials (B) and negative potentials (C). Each trace had a duration of 8 sec. (D) Probability of observing the open state as a function of voltage. The probability is defined as the count for the high-conductance state divided by all counts in the all-point histogram. (E) IV curve obtained for 10 individual NP pores. (F) Conductance histogram for 97 single NP channels recorded at a potential of -20 mV with a mean of 1.59 ± 0.07 nS.

DOI: 10.1038/NNANO.2015.279

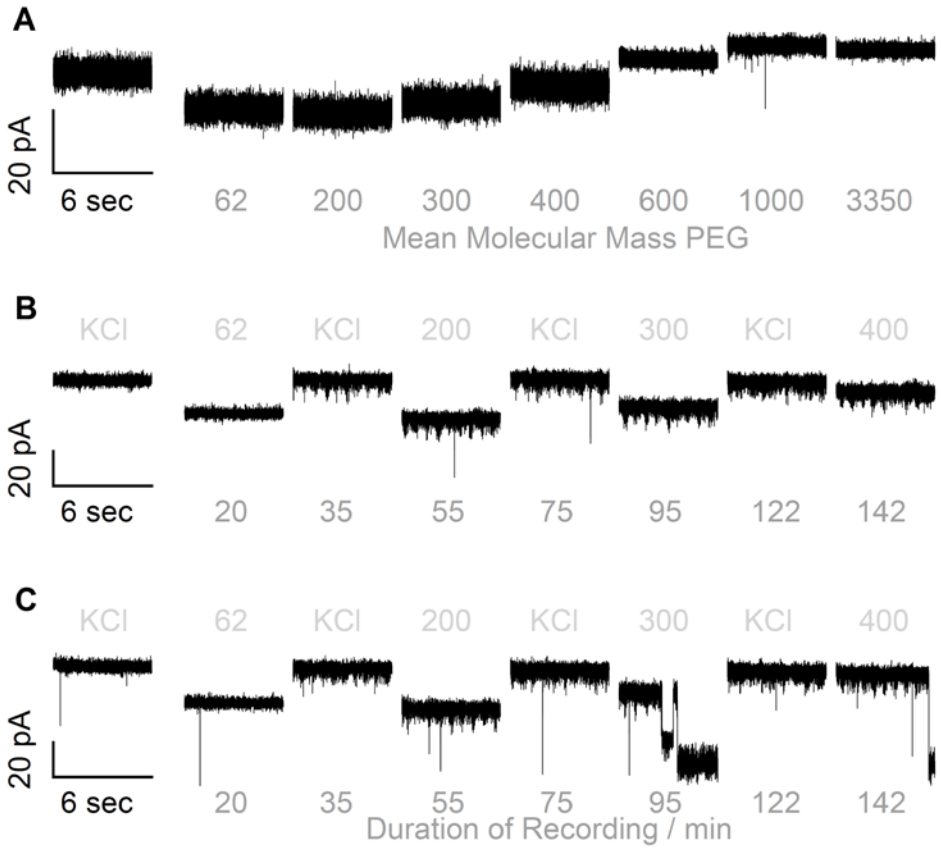


**Supplementary Fig. 7.** The diameter of the channel lumen of NP can be determined by recording the single-channel conductance in the presence of PEG molecules of different molecular masses. (A) Representative traces, recorded at +20 mV at the *cis* side and 1 M KCl, 10 mM HEPES pH 8.0, in the absence and presence of PEG molecules of molecular mass indicated below the trace segments. (B) and (C) show similar traces of one pore each recorded for a duration of up to 142 min, as indicated below the traces. The pores were exposed to electrolyte solution with PEG molecules of different molecular mass (indicated above traces) or to a KCl solution after washing out PEG to restore the initial pore current (indicated by KCl). The traces were recorded at +40 mV at the *cis* side. Short regular current downward reflections after 35 min with an amplitude of approximately 10 % of the main current are due to interfering external electrical noise. The lower current level in C at 95 min and 142 min reflects the rare temporary collapse of the pore in the presence of PEG.

### 2.5. FRET and gel electrophoretic analysis of key-induced transition of NP-C to NP-O

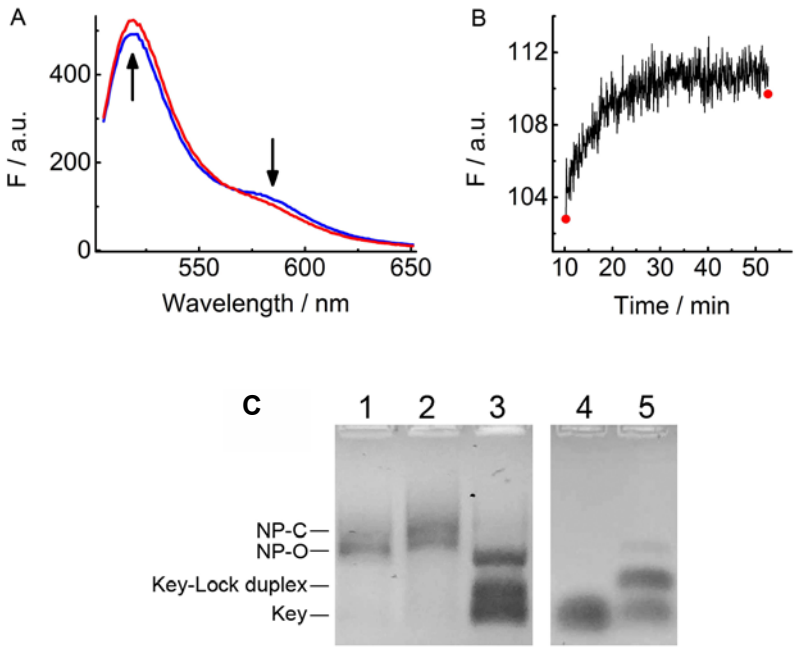


**Supplementary Fig. 8.** FRET and gel analysis confirms that key DNA triggers the removal of lock DNA from NP-C. (A) Fluorescence spectra of NP-C (blue line) and after addition of key DNA (red line), recorded at 1 μM NP-C in buffer A and the optional 5 molar excess of oligonucleotide key. Arrows indicate the increase in the signal of the donor which is attached to the pore and the decrease in the signal of the acceptor at the lock. Magnified FRET signals could have been achieved by decreasing the distance between the FRET fluorophore pairs and moving the acceptor closer to the docking site. But this might have perturbed the key-lock opening mechanism. (B) Kinetic trace for the fluorescence increase of the donor signal of NP-C upon addition of key as in panel A. The red dots at the left and right of the curve indicate the fluorescence signal of separately prepared NP-C and NP-O, respectively. The overlap between the end point of the trace and the NP-O signals confirms that key completely removes the lock. (C) 1.5% Agarose gel electrophoresis of cholesterol-free versions of NP-C (lane 1), NP-O (lane 2), and NP-C (lane 3) exposed to 5-molar excess of key oligonucleotide leading to the reversion back to NP-O. Key only (lane 4) and Key-Lock duplex with 5 molar excess key (lane 5) are also shown.

DOI: 10.1038/NNANO.2015.279

### 2.6. Voltage and orientation-dependent conductance of NP-O

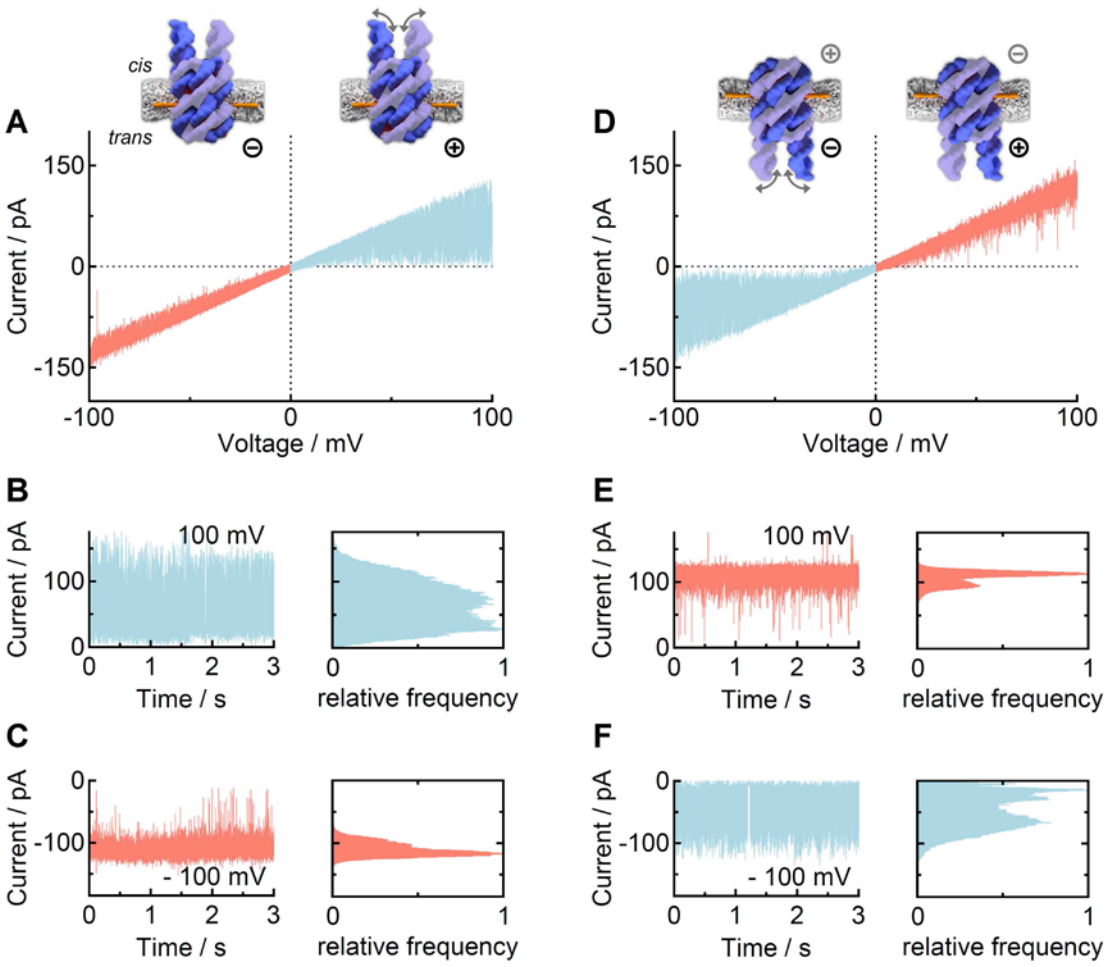


**Supplementary Fig. 9**. The conductance properties of NP-O display a voltage sign-dependent behavior in line with the asymmetric nature of the channel. The analysis reveals two classes which indicate that the pore can insert into the planar membrane in two different orientations. (A) Current trace for a voltage ramp from -100 to +100 mV of a *cis*-pore which is characterized by a quiet current at negative potentials and high-amplitude conductance variations at positive potentials. The conductance signature likely stems from a pore with the DNA docking sites positioned at the *cis* side of the membrane. At positive potentials, the negatively charged docking sites can be electrophoretically drawn towards the *trans* side, and the flapping into the channel entrance likely causes the current noise. The voltage polarity is shown at the membrane sides. The behavior was observed for 13 pores. (B, C) Current traces of a *cis*-pore of (A) at a constant potential of (B) +100 mV and (C) -100 mV. (D) Current trace for a voltage ramp from -100 to +100 mV of a *trans*-pore which is characterized by high-amplitude conductance variations at negative potentials and a quiet current at positive potentials. *Trans*-pores are inserted in the membrane in the opposite orientation to the *cis*-NP-O pore i.e. with the docking site at the *trans* side of the pore. The behavior was observed for 14 pores. (E, F) Current traces of a *trans*-pore at a constant potential of (E) +100 mV and (F) -100 mV. The current traces for *cis* and *trans*-NP-O pores are equal after inverting for the voltage sign and were hence combined in the analysis as shown in Supplementary Fig. 10.

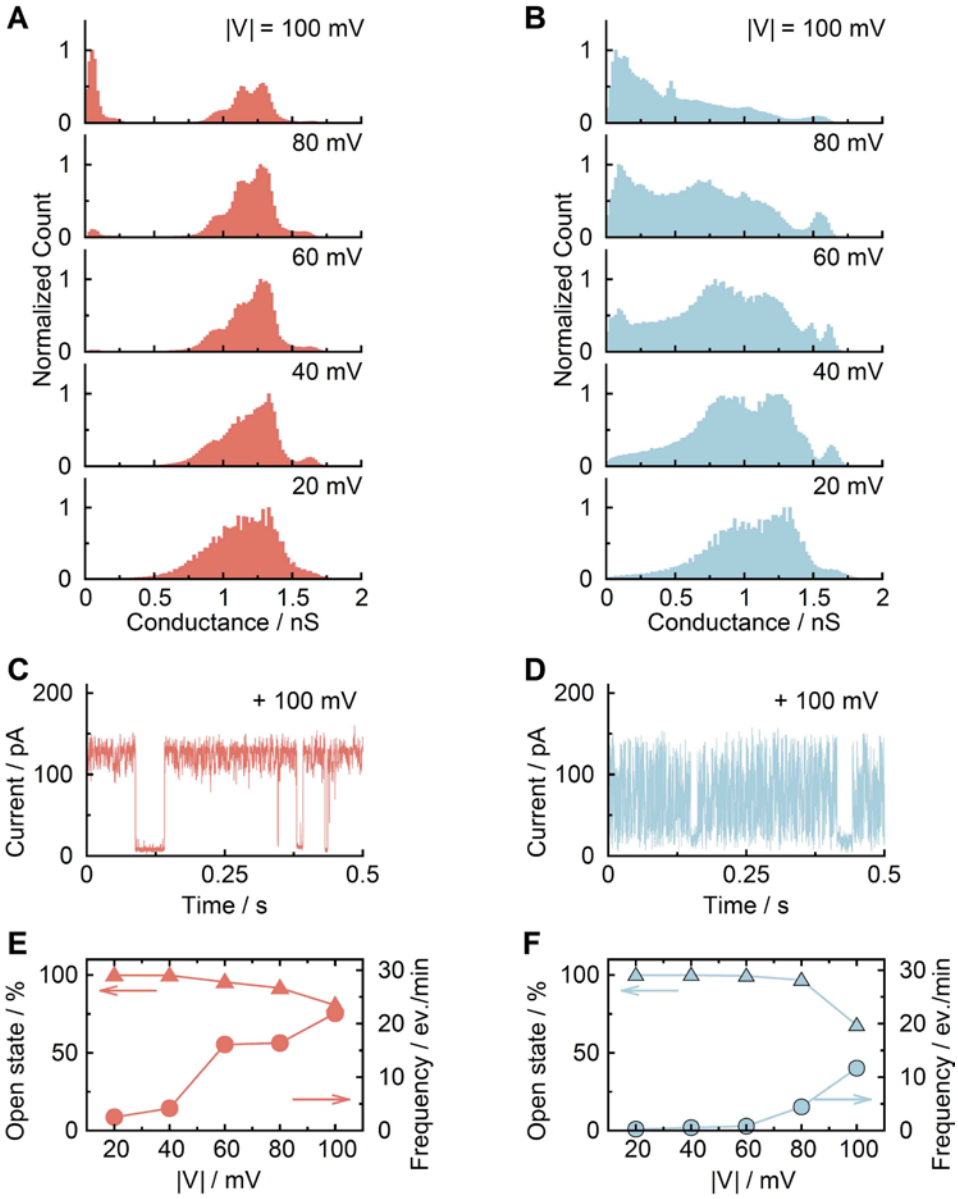


**Supplementary Fig. 10.** NP-O channels are open at voltages from +60 mv to -80 mV but can exhibit temporary pore closures at higher voltages. For the analysis, single-channel current traces were recorded at voltages in 20 mV steps from -100 to + 100 mV. In line with the symmetric conductance behavior of *cis* and *trans*-NP-O pores (as defined and color-coded in Supplementary Fig. 9), the corresponding data were combined. (A) All-point-histograms for red conductances corresponding to *cis*-NP-O traces from negative potentials and *trans*-NP-O traces at positive potentials. (B) All-point-histograms for blue conductances corresponding to *cis*-NP-O traces from positive potentials and *trans*-NP-O traces at negative potentials. The histograms in A and B are organized following the modulus of the potential. (C, D) Current traces of a single (C) *trans*-NP-O and (D) *cis*-NP-O pore at +100 mV displaying temporary and almost complete pore blockades i.e. gating events. (E, F) Voltage-dependent probability of the open state and the frequency of gating events for (E) red traces and (F) blue trace. The open state is defined in Supplementary Fig. 6. The analysis presented in A&B and E&F is based on data from single-channel current traces of 13 *cis*-NP-O and 14 *trans*-NP-O pores with each trace of 8 sec duration.

DOI: 10.1038/NNANO.2015.279

### 2.7. Conductance properties of NP-C

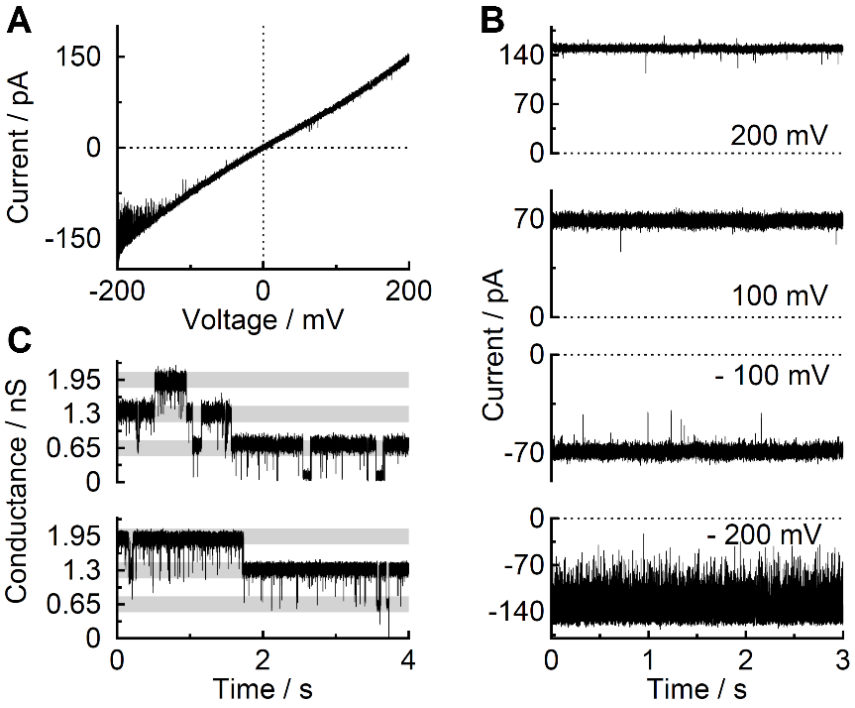


**Supplementary Fig. 11.** NP-C pores display ohmic behavior from -100 to +100 mV. They neither show voltage-sign dependent current fluctuations as NP-O, nor temporary current blockades as NP or NP-O. The higher stability is caused by the inclusion of the lock DNA strand and the extra stabilization between two duplex staves of the pore. (A) Current trace of a single NP-C pore for a voltage ramp from -200 to +200 mV. (B) Current traces of a single NP-C pore at the indicated voltages. (C) Traces of multiple simultaneous inserted pores held at -200 mV (top) and +180 mV (bottom). The high voltage leads to pore closures. The conductance bands of the pores are underlined in gray.

### 2.8. DLS analysis of vesicles

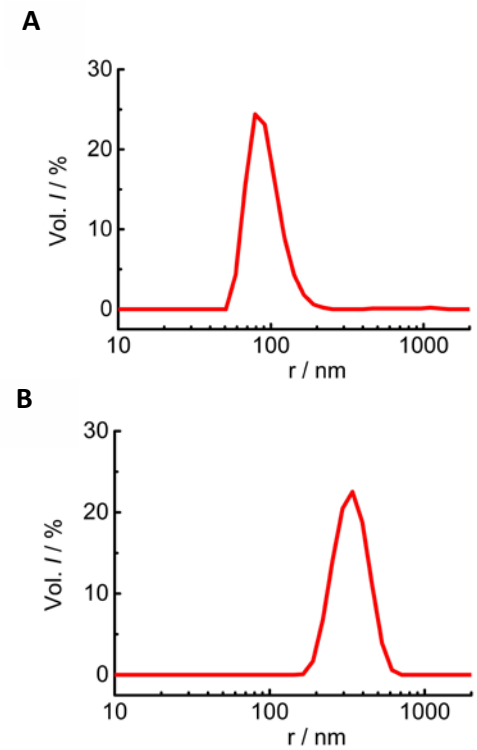


**Supplementary Fig. 12.** (A) Dynamic light scattering analysis of SUVs encapsulated with sulforhodamine B (50 mM) in buffer A used for release studies. (B) Dynamic light scattering analysis as in A but with of LUVs containing NP-C for the key-mediated release assay.

DOI: 10.1038/NNANO.2015.279

### 3.9. Control release experiment

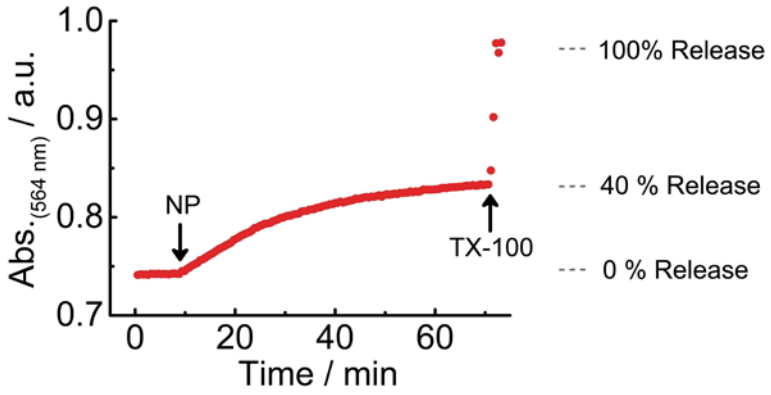


**Supplementary Fig. 13.** Monitoring the α-hemolysin-mediated release of sulforhodamine B encapsulated in SUVs. After 10 min of thermal equilibration, αHL (5 μL, 0.1 μM final protein concentration) was added to the SUV solution (1 mL, 50 mM SRB encapsulated into vesicles composed of PE:PC 30:70), as indicated by the downward arrow. Dye release was observed by an increase in the absorbance over 60 min. To determine the maximum amount of dye present in the SUVs, detergent Triton-X 100 (0.035 % w/v) was added to rupture all vesicles.